Confined Self-Assembly of Toric Focal Conic Domains (The Effects of Confined Geometry on the Feature Size of Toric Focal Conic Domains)

Yun Ho Kim,[†,||] Dong Ki Yoon,[†] M. C. Choi,[‡,§] Hyeon Su Jeong,[†] Mahn Won Kim,[‡] Oleg D. Lavrentovich,[||] and Hee-Tae Jung*,[†]

Department of Chemical and Biomolecular Engineering (BK-21), Korea Advanced Institute of Science and Technology, Daejeon 305-701, Korea, Department of Physics, Korea Advanced Institute of Science and Technology, Daejeon 305-701, Korea, Material Research Laboratory, University of California Santa Barbara, Santa Barbara, California 93106, and Liquid Crystal Institute and Chemical Physics Interdisciplinary Program, Kent State University, Kent, Ohio 44242

Received September 2, 2008. Revised Manuscript Received November 25, 2008

A smectic liquid crystal (LC) containing a rigid biphenyl group and semifluorinated chains exhibits a high density of toric focal conic domains (TFCDs) arranged in an ordered array when confined within a microchannel. The formation of the TFCDs is strongly influenced by the width (W) and depth (h) of the confined microchannels, most importantly, by the channel depth. We studied a broad variety of microchannels, with varying width in the range of 3−200 μm and depth in the range of 2−10 μm. The radius of the TFCDs increases with increases in the width until the saturated radius is achieved, which is determined by the depth of the channel. We used the elastic-anchoring model of TFCD formation to explain the experimental observations. The model allows one to trace the dependence of the TFCD radius on the channel depth h, to explain why the TFCDs do not form in channels that are too shallow or too narrow.

1. Introduction

Self-assembling materials such as colloids, block copolymers, supramolecular dendrimers, and surfactants have been shown to be extremely versatile in the generation of functional structures.[1−3] The aggregation of individual molecules into a final desired structure via self-assembly is currently one of the most exciting research areas in materials science and nanotechnology.[4] Self-assembly generally results in the formation of thermodynamically stable structures, so techniques based on self-assembly can be used to produce structures that are relatively defect-free and self-healing.[5−8]

We recently showed for the first time that highly regular arrays of toric focal conic domains (TFCDs) form in smectic A (SmA) liquid crystals (LCs) confined within surface-modified microsized channels.[9,10] The experimental observations related to the confinement of focal conic domains in small smectic slabs have been described by several authors since the first quantitative measurements by Fournier, Dozov, and Durand in 1990.[11] In addition, there are recent studies that are also concerned with confinement effects on focal conic domains achieved by Bramble et al., Guo et al., and Shahab-Shelly and Anna in a somewhat different geometry.[12−14] Direct visualization through scanning electron microscopy (SEM) demonstrated that the domain formation is driven by the hybrid character of surface anchoring, as the molecules prefer to align tangentially to the walls of the microchannel and perpendicularly to the free surface. A TFCD represents a system of curved layers folding around two linear defects, a central straight line, and a circular defect limiting the base of the TFCD. We demonstrated the concept of smectic LC lithography by trapping nanoparticles in the center of each TFCD, at the core of the axial defect.[10] This LC defect-base lithography is very different from the known approaches based on lithographically defined templates. The advantage is in its simplicity, short time needed to form the arrays of defects, and the possibility to control the geometry of the arrays through the geometry of confining microchannels. The latter is important, as the ability to control of the feature size and spacing is essential for applications in optoelectronics,[15,16] selective membranes,[17,18] creation of nanopatternied templates,[19,20] nanoelectronic machines, micro/nano-electromechanical (MEMs/NEMs) devices, and biochips/sensors.[21,22]

* To whom correspondence should be addressed. Tel.: +82-42-869-3931. Fax: +82-42-869-3910. E-mail: heetae@kaist.ac.kr.
† Department of Chemical and Biomolecular Engineering, Korea Advanced Institute of Science and Technology.
|| Kent State University.
‡ Department of Physics, Korea Advanced Institute of Science and Technology.
§ University of California Santa Barbara.

(1) Cao, G. *Nanostructures and Nanomaterials: Synthesis, Properties & Applications*; Imperial College Press: New York, 2004.
(2) (a) Cheng, J. Y.; Ross, C. A.; Smith, H. I.; Thomas, E. L. *Adv. Mater.* **2006**, *18*, 2505. (b) Kim, S. H.; Misner, M. J.; Xu, T.; Kimura, M.; Russell, T. P. *Adv. Mater.* **2004**, *16*, 226.
(3) Percec, V.; Glodde, M.; Bera, T. K.; Miura, Y.; Shiyanovskaya, I.; Singer, K. D.; Balagurusamy, V. S. K.; Heiney, P. A.; Schnell, I.; Rapp, A.; Spiess, H.-W.; Hudson, S. D.; Duan, H. *Nature* **2002**, *419*, 384.
(4) Whitesides, G. M.; Grzybowski, B. *Science* **2002**, *295*, 2418.
(5) Schaffer, E.; Thurn-Albrecht, T.; Russell, T. P.; Steiner, U. *Nature* **2000**, *403*, 874.
(6) Lu, Y.; Yin, Y.; Li, Z.-Y.; Xia, Y. N. *Nano Lett.* **2002**, *2*, 785.
(7) (a) Cheng, J. Y.; Mayes, A. M.; Ross, C. A. *Nat. Mater.* **2004**, *3*, 823. (b) Epps, T. H., III; Cochran, E. W.; Bailey, T. S.; Waletzko, R. S.; Hardy, C. M.; Bates, F. S. *Macromolecules* **2004**, *37*, 8325.
(8) Yoon, D. K.; Lee, S. R.; Kim, Y. H.; Choi, S.-M.; Jung, H.-T. *Adv. Mater.* **2006**, *18*, 509.
(9) Choi, M. C.; Pfohl, T.; Wen, Z. Y.; Li, Y. L.; Kim, M. W.; Israelachvili, J. N.; Safinya, C. R. *Proc. Natl. Acad. Sci. U.S.A.* **2004**, *101*, 17340.
(10) Yoon, D. K.; Choi, M. C.; Kim, Y. H.; Kim, M. W.; Lavrentovich, O. D.; Jung, H.-T. *Nat. Mater.* **2007**, *6*, 866.
(11) Fournier, J. B.; Dozov, I.; Durand, G. *Phys. Rev. A* **1990**, *41*, 2252.
(12) Bramble, J. P.; Evans, S. D.; Henderson, J. R.; Atherton, T. J.; Smith, N. J. *Liq. Cryst.* **2007**, *34*, 1137.
(13) Guo, W.; Herminghaus, S.; Bahr, C. *Langmuir* **2008**, *24*, 8174.
(14) Shojaei-Zaden, S.; Anna, S. L. *Langmuir* **2006**, *22*, 9986.
(15) Wang, X. D.; Summers, C. J.; Wang, Z. L. *Nano Lett.* **2004**, *4*, 423.
(16) O'Neill, M.; Kelly, S. M. *Adv. Mater.* **2003**, *15*, 1135.
(17) Percec, V.; Bera, T. K. *Biomacromolecules* **2002**, *3*, 167.
(18) Arora, G.; Sandler, S. I. *Nano Lett.* **2007**, *7*, 565.
(19) Jung, J. M.; Stellacci, F.; Jung, H.-T. *Adv. Mater.* **2007**, *19*, 4392.
(20) Cheng, J. Y.; Zhang, F.; Chuang, V. P.; Mayes, A. M.; Ross, C. A. *Nano Lett.* **2006**, *6*, 2099.
(21) Palacios, M. A.; Nishiyabu, R.; Marquez, M.; Anzenbacher, P., Jr. *J. Am. Chem. Soc.* **2007**, *129*, 7538.

10.1021/la802870z CCC: $40.75
Published on Web 01/09/2009

Scheme 1. The Model of Confined Geometry and LC Material[a]

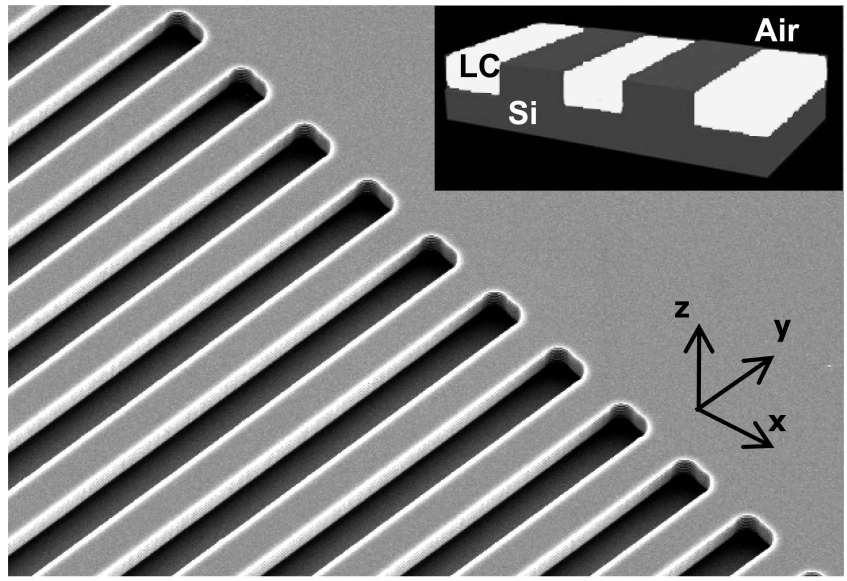

[a] Representative microchannel of 5 μm depth and width by SEM. (inset-top) Schematic representation of the space filling of the LC in the confined channel. (Bottom) The molecular structure, phases, and transition temperature of the semi-fluorinated smectic LC compound.

The goal of this study is to explore how the feature size and spacing in the TFCD arrays depend on the depth h and width W of microchannels hosting the SmA. We study a broad variety of microchannels, with W varying in the range of 3−200 μm and h in the range of 2−10 μm. The periodic arrays of energetically stable TFCDs form when both W and h are above some critical values, $W_c \approx 4$ μm, and $h_c \approx 3$ μm. The arrays represent two-dimensional (2D) close packings of TFCDs, with their bases at the bottom of the microchannel and apexes at the free surface of the SmA slab. To interpret the relationship between the geometrical features of TFCD arrays and the dimension of the microchannels, we employ the model of surface-induced TFCDs.[23]

2. Experimental Section

The microchannels with square cross-sections were fabricated on (100) silicon wafers with conventional photolithography and reactive ion etching techniques (Scheme 1). The channels we fabricated were 2, 5, or 10 μm deep, 3−200 μm wide, and 10 mm long. We chose a SmA material with rod-like molecules (4′-(5,5,6,6,7,7,8,8,9,9,10,10,-11,11,12,12,12-heptadecafluorododecyl-oxy)-biphenyl-4-carboxylic acid ethyl ester),[24,25] because this material was found to consistently yield hexagonal highly ordered patterns of TFCDs in the channels. The reason why this material produces better ordered TFCD lattices than other SmA materials with alkyl terminated LC molecules[26,27] is not entirely clear, but may be related to the semifluorinated nature of the chains present in the molecules.[24,25] To produce tangential surface anchoring of the SmA on the bottom substrate, a fluorinated polymer (Teflon-AF, Dupont) was spin-coated from solution in an organic fluorinated solvent (Fluorinert FC-77, 3M); the alignment material was not treated further after drying.

The crystalline powder of the SmA material was placed on the grooved substrate and then heated to the temperature corresponding to the isotropic phase (with a Mettler FP82 hot-stage and a Mettler FP90 controller) in order to fill these grooved substrates by capillary action. The amount of the dry powder was controlled in order to fill the channels completely. The sample was then cooled into the SmA phase (from 195 to 114 °C) at a rate of 10 °C/min (Scheme 1). The in-plane textures of the samples were observed with a polarizing optical microscope (POM) (Leica DMLB) equipped with a hot stage and charge-coupled device (CCD) camera. The content of the microchannels was also examined with field emission SEM (Serion FE-SEM, FEI, NNFC in KAIST) to determine the depth of the SmA samples and also the curvature of the layers. By using a well-controlled amount of the initial dry powder and the controlled sublimation of the material at elevated temperatures, we were able to produce samples in which the SmA film has a thickness practically equal to the depth of the channel. The samples for the SEM observations were prepared by fracturing them at room temperature. As the SmA phase is in a glassy state at this temperature, fracturing produces fresh interfaces that reveal the internal structure of the SmA distortions within the channels. The fractured samples were placed onto a carbon surface and then coated with Pt (10 nm) for better contrast and protection from the electron beam.

3. Results and Discussion

3.1. The Basic Features of TFCDs in a Confined Microchannel System. To produce periodic arrays of TFCDs, the samples were heated using a Mettler FP82 hot-stage and a Mettler FP90 controller to a temperature at which the material is in the isotropic phase, in order to fill the grooved substrates. The materials were then cooled at 5°/min to room temperature to produce the TFCDs. Upon cooling from the isotropic phase, the semifluorinated material directly transformed into an SmA phase (without a nematic phase) that is stable between 185 and 111 °C (see the Supporting Information, S1). The TFCD array is very stable through all scales of the channel geometry. The TFCD

(22) Wilson, D. S.; Nock, S. *Angew. Chem., Int. Ed.* **2003**, *42*, 494.
(23) Lavrentovich, O. D.; Kleman, M.; Pergamenshchik, V. M. *J. Phys. II (Paris)* **1994**, *4*, 377.
(24) Johansson, G.; Percec, V.; Ungar, G.; Zhou, J. P. *Macromolecules* **1996**, *29*, 646.
(25) Percec, V.; Johansson, G.; Ungar, G.; Zhou, J. P. *J. Am. Chem. Soc.* **1996**, *118*, 9855.
(26) Lee, S. R.; Yoon, D. K.; Park, S. H.; Lee, E. H.; Kim, Y. H.; Stenger, P.; Zasadzinski, J. A.; Jung, H.-T. *Langmuir* **2005**, *21*, 4989.
(27) Lee, E. H.; Yoon, D. K.; Jung, J. M.; Lee, S. R.; Kim, Y. H.; Kim, Y.-A.; Kim, G. C.; Jung, H.-T. *Macromolecules* **2005**, *38*, 5152.

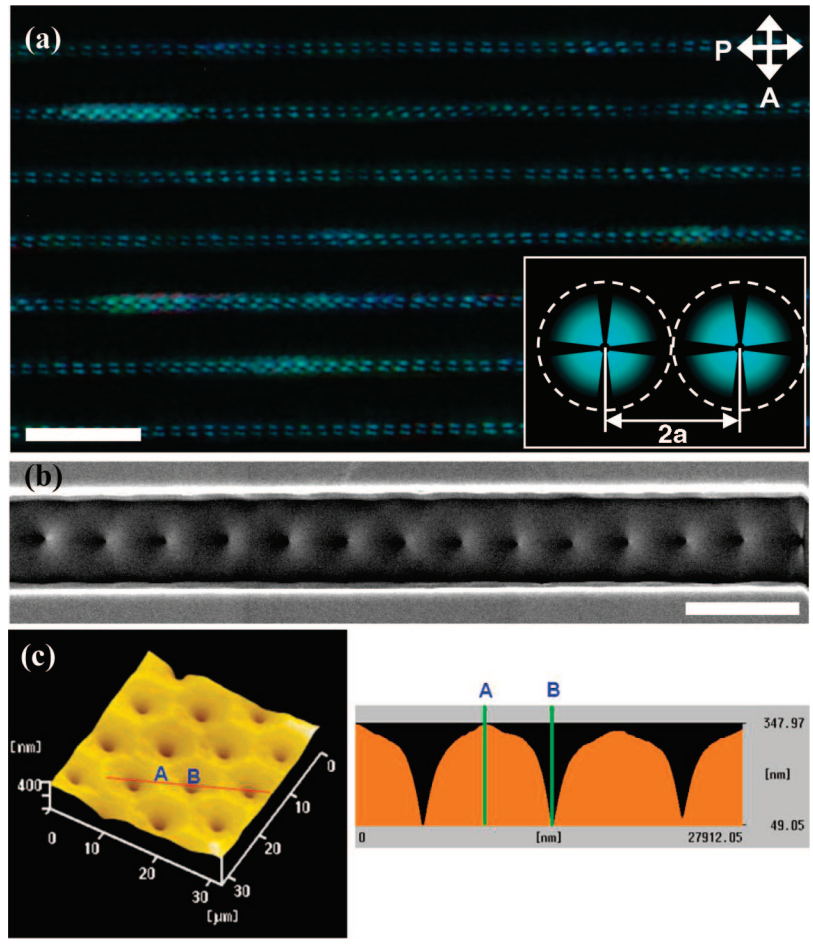

Figure 1. (a) The densely populated TFCDs in the microchannel. POM image of smectic LC material on Si microchannel of 5 μm width and depth (scale: 20 μm). Inset shows that schematic diagram of TFCDs as POM observation; the radius (a) of each TFCD is defined by half of the center-to-center distance between neighboring TFCDs. (b) The magnified SEM image of a linear TFCD array in the same microchannel (scale: 5 μm). (c) Atomic force microscope (AFM) three-dimensional (3D) topograph and height profile of a hexagonal TFCD array.

array starts to form in SmA phase, and it preserves at room temperature (soft crystal phase). The process of TFCD formation or nucleation was very fast, just taking several seconds. This might be due to the fast response time and high mobility of low molecular weight LCs. The TFCD structure had not changed up to this point, indicating thermodynamically stable TFCDs in the system. The molecules are perpendicular to the flexible SmA layers and showed no long-range order within the layers. In microchannels, the SmA phase forms ordered arrays of TFCDs. Further cooling results in the formation of an SmX phase with in-plane ordering of molecules and a crystalline phase (Scheme 1). The basic features of TFCDs such as the radius of base and the optical "Maltese cross" texture are preserved in the crystalline phase at room temperature, which allows us to use SEM and transmission electron microscopy (TEM) to further characterize the structures formed in the SmA phase at elevated temperatures.

The SmA films confined to the microchannels show a periodic regular pattern of circular domains extending over the entire length and width of the channels (Figures 1 and 2). Polarized optical microscopy (POM) shows that each TFCD produces a characteristic Maltese cross texture, indicating that the projection of the director field onto the plane of the substrate is radial within the area bound by the circular basis of the TFCD (Figure 1a). The TFCDs in most cases are in contact with each other, so that the radius (a) of an individual TFCD equals half of the center-to-center distance $2a$ between two neighboring TFCDs (Figure 1a, inset). This behavior is similar to that found in hard-

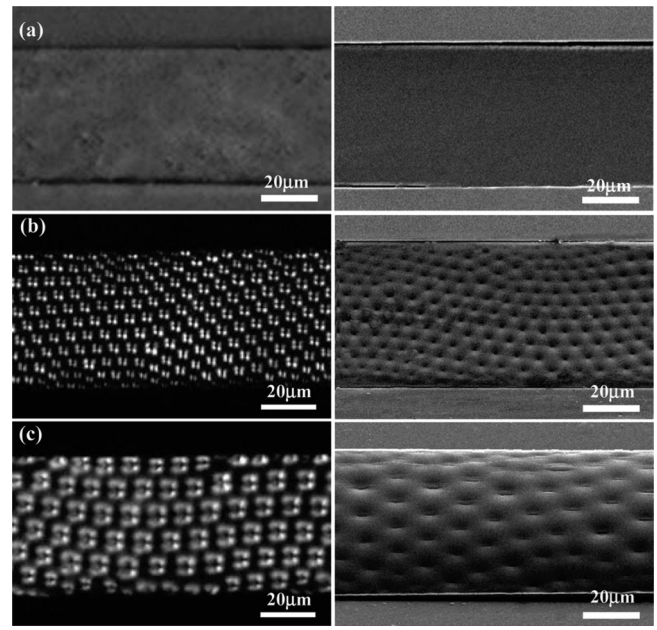

Figure 2. POM (left column) and SEM (right column) textures of TFCD arrays in microchannels of different depths $h = 2$, 5, 10 μm (from top to bottom) and fixed width $W = 50$ μm. The TFCDs do not form in the shallow channels of 2 μm depth. In panel a, a waveplate (530 nm) is inserted to enhance the weak contrast of the image.

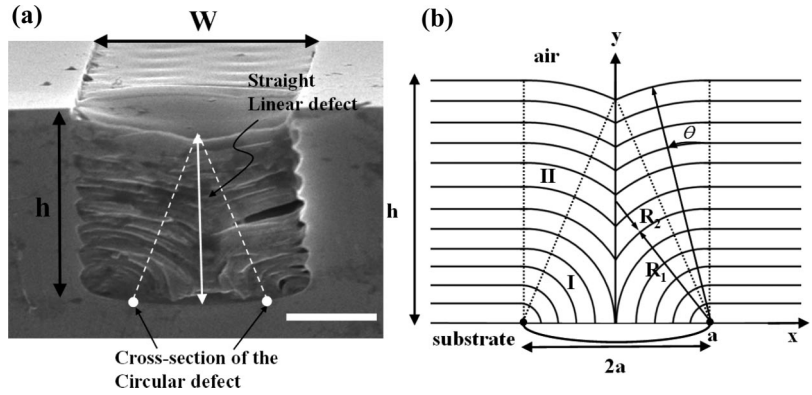

Figure 3. The geometry model of TFCD for free energy calculation. (a) SEM image of smectic material confined in a microchannel with 5 μm depth and width. Fractured SEM image directly shows the internal layered structure and circular curvature of layers in TFCD. Arrows indicate the pair of straight and circular defects (scales: 2 μm). (b) Geometry of TFCD in confined microchannel system based on panel (a).

sphere packing. According to the Friedel laws of association,[28−30] TFCDs cannot penetrate each other; the interactions of TFCDs are of a pure steric repulsion nature.

The characteristics of TFCD packing were determined using the fractured TEM method (see the Supporting Information, S2). The bluish green circles with white dotted lines indicate the birefringence regions of a few typical circular TFCDs. In POM, the dark background between the TFCD circles corresponds to zero birefringence and thus indicates that the smectic layers outside the TFCDs are parallel to the substrate (Figure 1a, inset). SEM micrographs (Figure 1b) further confirm that these toroidal domains are arranged in periodically ordered arrays; this particular image in Figure 1b is taken for a channel with $W = 5$ μm and $h = 5$ μm; only one row of the TFCD is formed in this narrow channel, and the average center-to-center spacing of the TFCD is 2.5 μm. Detailed investigation of the SmA−air interface with an AFM shows that each TFCD is associated with a depression of ∼300 nm in the center of the domain (Figure 1c). The depression structure at the core region of TFCD was investigated, in detail, in a confined system by Guo et al. and Designolle et al.[13,31] The height gradient is nonzero throughout the entire circular area occupied by the TFCD. SEM, Figures 2 and 3, demonstrates that the depressions are associated with bend of the SmA layers around the axial defect core of the TFCD. The AFM texture in Figure 1c was obtained for a channel of width $W = 100$ μm and depth $h = 10$ μm.

3.2. Relation between Microchannel Geometry and Radius of TFCDs by Microscopic Observation. We now proceed to the detailed experimental study of how the TFCD arrays depend on the thickness h and width W of the confining microchannels. Figure 2 shows POM and SEM images of ordered domains of the TFCDs in templates with the channel depth h varied from 2 to 10 μm. The channel widths is fixed, $W = 50$ μm. To characterize how well the channels are filled with the SmA material, we used SEM (Figure 3). As seen from the cross-sectional SEM images (Figure 3a and Supporting Information S3), the SmA material fills the entire depth of the channel. However, the top surface of the SmA film is not flat. First, the triple line, where the SmA, side wall, and air meet, is associated with a meniscus that extends through the entire length of the channel. Therefore, the film is somewhat thinner at the center of the channel as compared to the thickness near the walls (see the Supporting Information S3.) Second, each TFCD is associated with a pronounced depression at the apex of the TFCD. Comparing the AFM and SEM textures (Figures 1c and 3a), one concludes that the depression is a simple result of the layers bent around the central defect line in the domain structure; the layers are still tangential to the free surface (Figure 3a) and do not cross it (see the model in Figure 3b).

Figure 3a,b also illustrates the crucial feature of TFCD geometry: At the bottom and at the side walls, the molecules are aligned tangentially, while at the free surface they are aligned perpendicularly. These anchoring preferences are ultimately responsible for the formation of TFCD arrays. The layer curvatures are accommodated by two defect lines: a straight line perpendicular to the plane of the substrate, which serves as the axis of rotational symmetry of the TFCD, and a circular line at the bottom of the channel. Thus the overall internal structure of the domains observed with SEM agrees with the expected theoretical model[23] of a TFCD nucleated at the substrate that prefers tangential molecular alignment.

The average radius $\langle a \rangle$ of the TFCD shows a dramatic dependence on the microchannel depth h (Figure 2). TFCD arrays do not form at all if $h < 2$ μm (Figure 2a), but are found in $h = 5$ μm channels and channels with a larger depth (Figure 2a). The critical depth h_c below which the TFCDs do not form, therefore, is between 2 and 5 μm. In the channels with $h = 5$ μm and $W = 50$ μm, there are 9−10 parallel rows of TFCDs, the average radius of which is $\langle a \rangle = 2.6 \pm 0.2$ μm. In the channels with $h = 10$ μm, there are 5 or 6 parallel rows of TFCDs, with $\langle a \rangle = 5.3 \pm 0.2$. In other words, $\langle a \rangle$ increases with h.

Figure 4 shows POM and corresponding SEM images of TFCDs formed in channels of fixed depth $h = 5$ μm but different width W that varied from 3 to 100 μm. The TFCD arrays do not form in the narrow channel with $W = 3$ μm, but do appear for all other channels with $W \geq 5$ μm. In the microchannels wider than $W = 5$ μm, the number of rows of TFCD arrays increase as W increases. A single row of TFCDs with $\langle a \rangle = 1.25$ μm is observed for $W = 5$ μm, and arrays with 2−3, 4−5, 9−10, and 16−18 rows are found in channels with $W = 10$, 20, 50, and 100 μm, respectively (see the Supporting Information S4). The average radius of the TFCDs increases somewhat with W when W is in the range between 5 and 50 μm. For example, the average radius $\langle a \rangle$ of TFCDs increases to $\langle a \rangle = 1.8 \pm 0.2$ at $W = 10$ μm, and 2.6 ± 0.2 μm at $W = 50$ μm (Figure 5). For channels wider than $W_s \sim 50$ μm, the TFCD radius is practically independent of the width of microchannels. For example, we find $\langle a \rangle = 2.7$ μm for $W = 100$ μm, not much different than the values observed for

(28) Kleman, M. *J. Phys. (Paris)* **1977**, *38*, 1511.
(29) Blanc, C.; Kleman, M. *Eur. Phys. J. B.* **1999**, *10*, 53.
(30) Blanc, C.; Kleman, M. *Phys. Rev. E.* **2000**, *62*, 6739.
(31) Designolle, V.; Herminghaus, S.; Pfohl, T.; Bahr, C. *Langmuir* **2006**, *22*, 363.

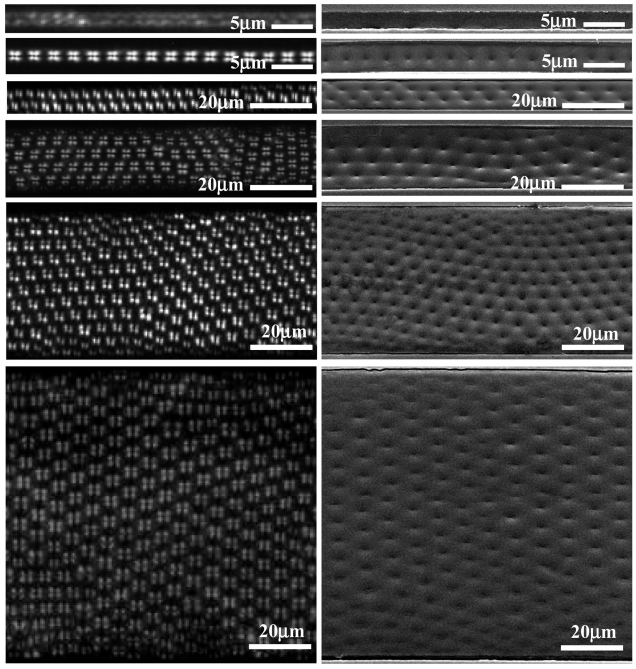

Figure 4. POM (left column) and SEM (right column) textures of TFCD arrays in microchannels of different widths $W = 3$, 5, 10, 20, 50, and 100 μm (from top to bottom) and fixed depth $h = 5$ μm. The SEM images are taken for samples tilted by 26° from the horizontal plane.

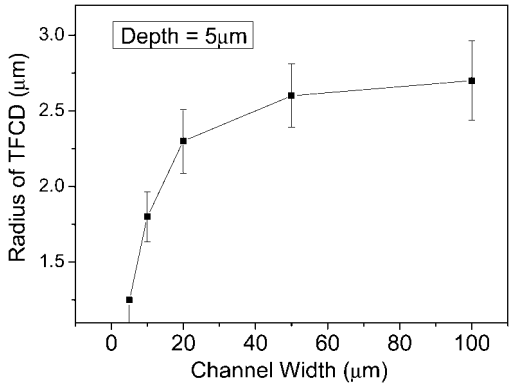

Figure 5. The experimental data for average TFCD radius as a function of the channel width with fixed depth of 5 μm. The average radius of TFCDs increases somewhat with small width ($W = 5-50$ μm) and saturates to a specific radius (~2.8 μm), which is almost half of the channel depth ($h = 5$ μm).

$W = 50$ μm (Figure 4). The data are based on the measurements performed for more than 100 domains for each width of the channel (Figure 4 and Supporting Information S5.) Note that the saturation value of $\langle a \rangle$, achieved in the channels much wider than $W_s \sim 50$ μm, is about $\langle a \rangle_{W\to\infty} = 2.8$ μm, which is of the same order as the depth of the channels studied ($h = 5$ μm). This correspondence is close to what is expected from the theoretical model[23] and its extension below.

3.3. The Free Energy Calculation for Theoretical Analysis. We now consider the analytical description of a TFCD. The stability of a TFCD in a confined geometry is determined by the balance in the surface anchoring and elastic energies.[32] As can be seen in the textures in Figures 2−4, the molecules prefer to be parallel to the walls and perpendicular to the free surface of the SmA film. These boundary conditions can only be satisfied when the layers are bent. The equilibrium radius of the TFCD depends on the elastic constant of the smectic layers (K) and the surface energy anisotropy ($\Delta\sigma^{subs}$), i.e., the difference in the surface energy per unit area between the state with the molecules parallel to the substrate and the state with the molecules perpendicular to the substrate ($\Delta\sigma^{subs} < 0$, see ref 33). The geometry of microchannels leads to additional factors that can influence the geometry of TFCD arrays.

First, the meniscus that forms near the triple line and extends through the entire length of the microchannel makes the local thickness of the cell nonuniform. As the domain size should depend on the thickness of the film, this meniscus alone can contribute to the observed W-dependence of the domain size. The tilted geometry of the air−SmA interface in the meniscus region also inevitably leads to the formation of linear dislocations, as discussed by Caillier and Oswald.[34] The shape of the meniscus is a complex problem, even if the side walls were extended to infinity (an infinite channel's depth h).[35] In our case, the problem is further complicated by the fact that the meniscus ends at the edge of the side wall, and its structure is not necessary equilibrium. On the other hand, the observed nonuniformity of the local thickness of SmA film is not very significant, since the variations in the film thickness across the channels represent less than 5% of the value of h (Supporting Information S4). At very large W ($\gg h$, a), the effect of meniscus on the average size of TFCDs should become negligible.

The second effect associated with the free surface is that of the surface depressions that develop at the apex of each TFCD. These depressions increase the area of the air−SmA interface with the surface tension coefficient $\sigma_{\perp}^{air}$; the corresponding increase of the surface energy should destabilize the TFCD. In addition, the SmA material that is removed by the depression, should be redistributed through the rest of the system, as the total volume of the SmA film should be preserved regardless of the presence of TFCDs. The depressions will raise the area of contact between the side walls and the SmA. If the channels are narrow and contain only a few rows of TFCD, this effect would be of importance, but in wide channels ($W \gg h$), the influence of this effect on $\langle a \rangle$ can be neglected.

The third effect of confinement geometry is through the requirement of commensurability between the lattice period of the TFCD array and the width of the channel. As predicted by the model,[23] at a given film thickness h, each isolated domain has an equilibrium radius determined by the h, elastic, and surface material parameters. Since each TFCD reduces the total free energy of the system, the most favorable arrangement of the TFCDs should be a hexagonal 2D packing of their circular bases at the bottom of microchannels. However, such an ideal arrangement is possible only when the lateral dimension of the SmA sample is infinite. In the bounded samples, the side walls set restrictions on how many full rows of TFCDs can fit into the channel. This confinement effect also influences the size of the domains if the ratio W/a is not very large. In what follows, we account for the effect of meniscus near the apex of each TFCD by calculating the corresponding area increase of the SmA−air interface. All other menisci effects are neglected, as the most important qualitative features are grasped by the dependence $a(h)$, while the experimentally observed dependence $a(W)$ is primarily due to the superposition of the local thickness effect and the packing problems of TFCDs.

(32) Kleman, M.; Lavrentovich, O. D. *Soft Matter Physics: An Introduction*; Springer: New York, 2003.

(33) Lavrentovich, O. D. *Sov. Phys. JETP* **1986**, *64*, 984.
(34) Caillier, F.; Oswald, P. *Phys. Rev. E* **2004**, *70*, 031704.
(35) Geminard, J. C.; Oswald, P. *Phys. Rev. E* **1997**, *55*, 4442.

In our model (Figure 3b), the domain is smoothly embedded into the matrix composed of flat horizontal layers. In the central part of the domain, the smectic layers are reoriented by an angle of $\pi/2$ with respect to the outside layers. The region of deformation is restricted by the cylindrical surface. The smectic layers are distorted inside a cylindrical volume with a radius $a \ll W$ and a height $h \ll W$, assumed to be equal to the channel's depth. The packing of circular bases of TFCDs at the bottom of the microchannels is hexagonal, as dictated by the hard-core repulsive interactions.

The free energy of domain formation can be expressed as the difference $\Delta F = F_e + F_s - F_0$ between the total energy of the defect state (composed of the elastic energy F_e and the surface energy F_s) and the energy F_0 of the reference uniform state with flat layers:

$$F_0 = \pi a^2(\sigma_\perp^{air} + \sigma_\perp^{subs}) \quad (1)$$

Here, $\sigma_\perp^{air}$ and $\sigma_\perp^{subs}$ are the surface energies per unit area at the SmA−air interface and at the bottom plate when the molecules are aligned perpendicularly to it, respectively. Using the results for F_e and F_s obtained in the Supporting Information S6, S7, one arrives at the free energy of TFCD formation, expressed as a function of the dimensionless TFCD radius $\rho = a/h$:

$$\Delta F = F_e + F_s - F_0 = 2\pi Kh\rho\left(\ln\frac{h\rho}{\xi} - 2\right)\left(\frac{\pi}{2} - \theta^*\right) + \pi Kh\rho\theta^* \ln\frac{h\rho}{\xi} + 4\pi Kh\left(\sqrt{1-\rho^2} - 1\right) + \pi Kh\rho\int_0^{\theta^*} \ln(\rho - \sin\theta)\mathrm{d}\theta - 2\pi Kh\rho\int_{\theta^*}^{\pi/2} \ln(\sin\theta)\mathrm{d}\theta - \pi h^2\rho^2\bar{K} + 2\sigma_\perp^{air}\pi h^2\left\{\sqrt{1-\rho^2} - 1 + \rho\,\mathrm{arctg}\frac{\rho}{\sqrt{1-\rho^2}}\right\} + \pi h^2\rho^2\left(\Delta\sigma^{subs} - \sigma_\perp^{air}\right) \quad (2)$$

where ζ is the cutoff of the elastic energy integration,[23] defining the core radius of the defects, K is the splay elastic constant of SmA, $\Delta\sigma^{subs} = \sigma_\parallel^{subs} - \sigma_\perp^{subs} < 0$, and $\sigma_\parallel^{subs}$ is the surface energy per unit area for parallel molecular orientation at the SmA−substrate interface. The dimensionless radius ρ can be treated as an order parameter of the transition. For the uniform state, $\rho = 0$ and $\Delta F = 0$.

Figure 6a shows the variation in the free energy $\Delta F = \rho$ for a TFCD in microchannels of different depth h, as calculated using eq 2 with $K = 5 \times 10^{-11}$ N, $\bar{K} = 0$, $\xi = 3 \times 10^{-9}$m,[19] $\Delta\sigma^{subs} = -1.2 \times 10^{-3}$ N/m,[36,37] and $\sigma_\perp^{air} = 20 \times 10^{-3}$ N/m.[38] Note that K is assumed to be about 5 times larger than that for general alkyl-terminated SmA materials such as 8CB,[23,36] to reflect the fact that the fluorinated LC molecules are more rigid than other LCs due to the fluorinated moiety in the tail group.[39,40] This assumption is not critical, as smaller values of K produce similar results, especially if the surface tension anisotropy ($\Delta\sigma^{subs}$) is also adjusted.

The dependence $\Delta F(\rho)$ in eq 2 is nonmonotonous, with a minimum at $\rho = 0$ and another minimum at some nonzero $\rho^* > 0$. The first minimum corresponds to the defect-free state, and the second minimum corresponds to the TFCD of size $\rho^* > 0$. These two minima are separated by an energy barrier. These qualitative features are the same as described previously in ref

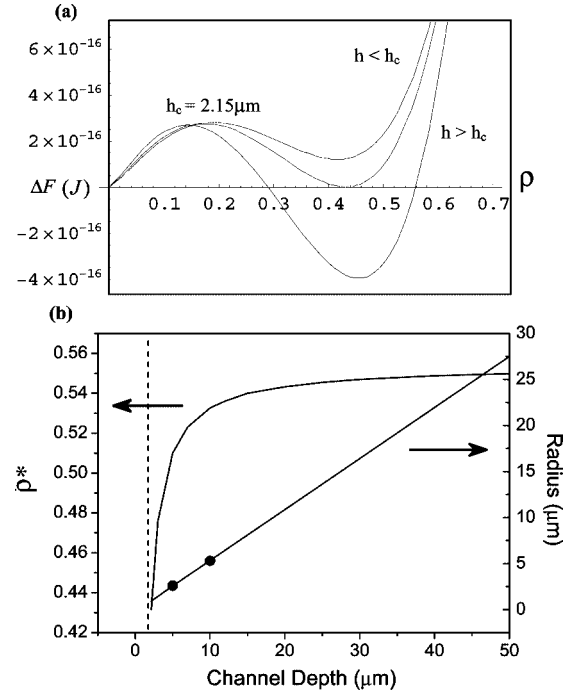

Figure 6. The effect of the channel depth h on the TFCD dimensionless radius $\rho = a/h$. (a) TFCD energy versus ρ for three different channel channel depths h (h = 2, 2.15, and 2.5 μm). The two minima of the energy are located at $\rho = 0$ and at a nonzero $\rho = \rho^*$. (b) The dependencies of ρ^* and a^* on the channel depth h. Dotted line indicates the limit of channel depth available for forming TFCD, which is the calculated critical channel depth (h_c = 2.15 μm). The two black spheres on the radius graph indicate measured radii at $h = 5$ μm ($\langle a\rangle \approx 2.6 \pm 0.2$ μm) and $h = 10$ μm ($\langle a\rangle \approx 5.3 \pm 0.2$) channels from experimental results.

19 for a TFCD bounded by two flat plates, and in the work by Fournier et al.[11] for the SmA slab with one free surface, at which the surface energy term was calculated as $(\pi\sigma_\perp^{air}a^4)/(12h^2)$. Figure 6a explains the essential features of the properties of the TFCDs in channels, as described below.

There is a critical channel depth h_c below which the TFCDs cannot be stable because the energy of any defect state with a nonzero a is larger than 0, the energy of the defect-free state. At $h = h_c$, the two energies become equal to each other, and at $h > h_c$, the TFCD energy becomes negative. With the parameters chosen for Figure 6a, we find that $h_c = 2.15$ μm, which is in good agreement with the experimental results ($2\,\mu\mathrm{m} < h_{cexp} < 5\,\mu\mathrm{m}$).

For channels deeper than the critical length, $h > h_c$, the function $\Delta F(\rho)$ has a minimum for a macroscopic value a^* of the domain radius. The latter is determined by the balance of the surface energy gain $\tilde{a}^2\Delta\sigma^{subs}$ and the elastic penalty $\tilde{a}K$ associated with the formation of the TFCD; the equilibrium radius of the domain should be on the order of[33]

$$a^* \sim K/|\Delta\sigma^{subs}| \quad (3)$$

Smaller TFCDs are unstable because the surface anchoring energy gain at the base of the FCD is not sufficient to overcome the elastic energy penalty associated with the curvature of the layers and defects. Note that there is always an energy barrier separating the states with $a = 0$ and $a = a^*$, which is a typical feature of the nucleation process. This energy barrier is usually too large to be surmounted by thermal fluctuations ($\tilde{k}_BT$); in real systems, the barrier can be overcome if TFCD nucleation occurs at mechanical irregularities such as surface irregularities (see ref 23 for a detailed discussion).

(36) Hinov, H. P. *J. Phys. (Paris)* **1981**, *42*, 307.
(37) Li, Z.; Folks, W. R.; Lavrentovich, O. D. *Proc. SPIE: Liq. Cryst. Mater., Devices, Appl. III* **1994**, *2175*, 21.
(38) Lavrentovich, O. D.; Tarakhan, L. N. *Poverkhnost* **1990**, *1*, 39.
(39) Eaton, D. F.; Smart, B. E. *J. Am. Chem. Soc.* **1990**, *112*, 2821.
(40) Jung, H.-T.; Coldren, B.; Zasadzinski, J. A.; Iampietro, D. J.; Kaler, E. W *Proc. Natl. Acad. Sci. U.S.A.* **2001**, *98*, 1353.

The equilibrium dimensionless radius $\rho^* = a^*/h$ corresponding to the minimum of $\Delta F(\rho)$ increases with h and then saturates (Figure 6b). The same dependence, replotted as $a^*(h)$ shows that the TFCD size increases with h almost linearly, as in the experiment. The model predicts $\rho^* = 0.51$, or $a^* = 2.55$ μm for a channel of depth $h = 5$ μm, and $\rho^* = 0.53$, or $a^* = 5.32$ μm for a channel of depth $h = 10$ μm, in agreement with the experimentally measured $\langle a \rangle \approx 2.6 \pm 0.2$ μm at $h = 5$ μm, and $\langle a \rangle \approx 5.3 \pm 0.2$ μm at $h = 10$ μm (Figures 2 and 6b).

The model above describes the depth dependence of the TFCD size and thus the periodicity of the TFCD arrays in the assumption that the width of the microchannels is large as compared to h. For relatively narrow channels, the domain size would also be influenced by the value of W, through the effects of menisci and through the commensurability of W and a. Further studies to quantify these effects are in progress.

4. Conclusions

In summary, we have investigated stable and regular TFCDs arrays that form when an SmA material is placed in confined microchannels that impose antagonistic orientational anchoring at the walls and at the free surface of the smectic material and thus act as nanotemplates. We used a semifluorinated material that has a highly ordered SmA LC phase because of the rigid fluorinated moiety in its constituent molecules. First, we used direct visualization of the finely layered structure of a TFCD in a microchannel to verify that the smectic layers, which are aligned normal to the side wall and parallel to the top surfaces, merge with the circular profile on the bottom wall surface. Second, we showed that the formation of the TFCDs is strongly influenced by the width and depth of the microchannels, most importantly, by the channel depth, h. The radius of the TFCDs increases with increases in the width until the saturated radius is achieved, which is determined by the depth of the channel. Finally, we used the elastic-anchoring model[19] of TFCD formation to explain the experimental observations. The model allows one to trace the dependence of the TFCD radius on the channel depth h, to explain why the TFCDs do not form in channels that are too shallow or too narrow. The ordered TFCD array structures produced with a smectic LC in a confined geometry with the possibility of size control might find new applications in fields such as nanotemplates, photonics, or microfluidics.

Acknowledgment. This work was supported by the National Research Laboratory Program of the Korea Science and Engineering Foundation (KOSEF), the Basic Research Program (R01-2005-000-10456-0), the KRF (D00078), and the CUPS-ERC program. X-ray experiments were carried out at the PLS with the partial support of MOST and POSCO. SEM experiments were executed at the NNFC. O.D.L acknowledges the support of an NSF DMR grant (0504516).

Supporting Information Available: (1) POM texture of LC material, (2) surface topography and fractured TFCDs, (3) the height difference between microchannel and smectic film, (4) the number of TFCD parallel rows as a function of channel width, (5) the measured radius of TFCD as a function of channel width with standard deviation, (6) calculation for free elastic energy of TFCD (F_e), (7) calculation of the surface energy (F_s), and (8) detailed experimental section. This material is available free of charge via the Internet at http://pubs.acs.org.

LA802870Z